Diamond & Related Materials 149 (2024) 111537

Contents lists available at ScienceDirect

Diamond & Related Materials

journal homepage: www.elsevier.com/locate/diamond

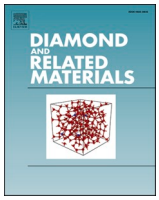

Enhancing mechanical and corrosion properties of GO and Al2O3 reinforced Cu composite coatings

Sezer Tan [a,*], Melisa Köse [a], Hasan Algül [a], Mert Aydin [b], Miraç Alaf [e], Ahmet Alp [a], Hatem Akbulut [a,c,d], Mehmet Uysal [a,c]

[a] Sakarya University, Faculty of Engineering, Department of Metallurgy and Materials Engineering, 54187, Sakarya, Turkey
[b] Altınok Galvanokimya, 34890 İstanbul, Turkey
[c] Sakarya University, Sakarya University Research and Development Center (SARGEM), Esentepe Campus, 54187, Sakarya, Turkey
[d] NESSTEC Energy & Surface Technologies A.S., Technology Development Zones, 54050, Sakarya, Turkey
[e] Department of Metallurgical and Materials Engineering, Bilecik Şeyh Edebali University, 11230 Bilecik, Turkey

ARTICLE INFO

Keywords:
Electroless coating
Nanorolls
Nanomechanical properties
Hybrid nano composite

ABSTRACT

Despite their significant functions and properties, the performance characteristics of Al_2O_3 ceramic particles and graphene oxide (GO) within hybrid copper composite coatings have been seldom investigated. This study successfully fabricated a Cu-GO- Al_2O_3 composite coating featuring fine particulate spherical network-like structures on St37 low carbon steel using an ultrasonic-electroless coating method. The effects of Al_2O_3-decorated graphene oxide hybrid reinforcement on the texture and nanomechanical properties of the copper matrix were examined. The tribological performance of the Cu-GO- Al_2O_3 composite coating under dry sliding conditions was evaluated, and the wear mechanism was investigated in detail. Results demonstrate that the Cu-GO- Al_2O_3 composite coating effectively reduces the wear rate and friction of the GO/ Al_2O_3 hybrid reinforced composite coating. Potentiodynamic polarization tests indicated that the Cu-GO- Al_2O_3 composite coating exhibits higher corrosion resistance compared to the copper matrix. The enhanced mechanical, tribological, and corrosion properties of the Cu-GO- Al_2O_3 composite coating are primarily attributed to: (i) the fine particulate spherical network-like structure; (ii) the synergistic effect of the GO and ceramic particle hybrid with a decorated structure; (iii) the formation of graphene oxide/ Al_2O_3 nanorolls in tribofilms and the excellent self-lubrication properties of graphene oxide. The Cu-GO- Al_2O_3 composite coating significantly improves the frictional and electrochemical properties of the copper matrix, offering new perspectives for next-generation electrical contacts and nano-electromechanical systems.

1. Introduction

Copper and copper alloys are widely used in frictional components, automotive micro-nano electronics and nano-devices, power materials, bushings, and electrical contacts due to extraordinary thermal conductivity (400 W/mK), electrical conductivity(58 MS/m), corrosion properties [1,2]. However, pure copper had already limited its wide application due to weak relative strength, hardness, and wear resistance. Furthermore, with the rapid development of the automobile and nano-device industries, there is a high demand for new materials with enhanced friction and electrochemical properties that maintain high electrical conductivity [3,4]. Therefore, designing wear and corrosion-resistant copper composite coatings is important for high-performance nano-devices.

Composite materials can be produced by different methods such as ball-milling, FSM etc. [5–7]. Electroless coatings are a coating technique that has been used for many years. Especially in the last fifty years, it has come to the fore with its excellent corrosion and wear resistance [8]. Electroless coatings allow many metals such as nickel and copper to be used as a matrix. In addition, it is very suitable for producing composites, which makes this technique stand out [9]. Currently, reinforcements, such as molybdenum sulfide (MoS_2) [10], GO [11,12], ceramic particles [13], are incorporated into the metal matrix to improve the tribological or corrosion properties. GO with a layered structure as reinforcement into metal matrix has attracted great attention due to low friction and high wear performance, anti-corrosion

* Corresponding author.
E-mail address: sezertan@sakarya.edu.tr (S. Tan).

https://doi.org/10.1016/j.diamond.2024.111537
Received 12 June 2024; Received in revised form 22 August 2024; Accepted 26 August 2024
Available online 28 August 2024

properties, and specific surface area [14,15]. As a corrosion inhibitor in metal deposition, graphene has excellent barrier properties against corrosive media. Moreover, the ultra-thin lamellar structure makes GO easy to permeate the contact interface for inhibiting direct contact metal-metal [16]. Fanyan et al. [17] studied the effect of graphene on the hardness, friction and wear of Cu-GO coating produced by spark plasma sintering method. It was displayed that the tribology and friction properties of the Cu-GO composite was improved by incorporating GO. Mai. [18] prepared copper-graphene oxide composite coating by electrodeposition. Compared with copper, the hardness was increased, contributing to improved friction and wear resistance. Baoyin [19] incorporated GO in the copper to significantly improves the corrosion resistance of the composites. However, its high incorporation and bad dispersion in coating adversely affect the metal matrix's friction, wear, and corrosion properties. To achieve a notable increase in tribological and anti-corrosion performance, graphene oxide must be combined with other reinforcements. Therefore, many reports have shown that the hybrid composite materials are an ideal reinforcement for nano metal matrix composites because they can provide a synergistic effect among each reinforcement in the matrix and be beneficial to the dispersion and interfacial combination between them reinforcement and matrix [20–27]. Lailesh et al. [28] reported that Cu xGnP/MWCNT(multi-walled carbon nanotube) hybrid composites improve wear resistance due to exposed rich carbon layer on the wear surface. Dong et al. [29] investigated physico-mechanical properties of Cu-graphene matrix composites decorated with tungsten carbide, demonstrating yield strength and ultimate tensile strength have enhanced up to 112 % and 72 %, respectively, when compared with those of Cu matrix.

So far, relevant research has mainly focused on the effects of graphene on the wear and corrosion properties of the copper matrix. To the best of our knowledge, there is currently no study reporting on the nanomechanical, friction, wear, and corrosion behaviors of the copper composite coatings reinforced by graphene oxide and Al_2O_3 ceramic particles. Therefore, this study aims to investigate the morphological, electrochemical and nanomechanical properties (hardness and elastic modulus) of Cu-Graphene Oxide-Al_2O_3 composite coatings, which exhibit superior tribological and corrosion resistance. These coatings were prepared using the ultrasonic-assisted electroless coating process and applied to St37 low carbon steel. While the Al_2O_3 was selected for its ability to enhance the mechanical strength of the coating through increased surface hardness, the GO reinforcement were preferred for their lubricating properties, their ability to improve wear and corrosion resistance, and their contribution to reducing surface roughness. Moreover, the present research further seeks the effect of nanoroll formation on the wear and friction performances of the copper composite coating reinforced by graphene oxide and Al_2O_3 ceramic particles.

2. Experimental

2.1. Fabrication of Cu-GO-Al_2O_3 composite coatings

According to our previous report, graphene oxide was synthesized by an improved Hummers method [30]. The thickness of graphene oxide (wall thickness) is 6–8 nm and the nominal particle size (surface area) of graphene oxide is between 2 and 6 μm. The electroless plating was carried out in a cell placed in a thermostatically controlled bath. The plating bath was ultrasonically stirred during deposition. Ultrasonic agitation was used for homogeneous dispersion and deagglomeration of graphene oxide and ceramic particles in the electrolyte during the deposition. The size of the Al_2O_3 (aluminum oxide) particles (CAS No: 1344-28-1, Sigma Aldrich) was approximately 50–100 nm which used as reinforcement in this study. The pH value was maintained at 9–9.5 and the temperature was kept at 65 °C. The bath compositions and the parameter for electroless copper composite coatings are displayed in Table 1. The low carbon steel (St37, chemical composition; C (0.11 wt %), Si (0.03 wt%), Mn (0.56 wt%), P (0.007 wt%), S (0.005 wt%), Cr (0.07 wt%), Ni (0.03 wt%)) used as substrates were pretreated by polishing with silicon carbide (SiC) papers, then cleaned in acetone followed by degreasing in alkali solution. Before coating the substrate subject to a treatment process that consisted of various steps such as sensitization and activation treatments: (1) The polished specimens were pickled in a 2 M solution of nitric acid (HNO_3) (2) Sensitization was carried out by ultrasonication in a bath containing 10 g/L $SnCl_2$ and 100 mL/L HCl for 20 min (3) activation was performed by ultrasonication in a bath containing 0.25 g/L palladium chloride ($PdCl_2$) and 3 mL/L hydrochloric acid (HCl) for 30 min. Between every step, the samples were rinsed in distilled water. The production process of composite coating is shown in Fig. 1.

Table 1
Bath composition and operating parameters for fabrication of composite coatings.

Composition	Cu	Cu-Al2O3	Cu-GO	Cu-GO-Al2O3
CuSO4·5H2O	10 g/L	10 g/L	10 g/L	10 g/L
Na3C6H5O7·2H2O	20 g/L	20 g/L	20 g/L	20 g/L
H3BO3	15 g/L	15 g/L	15 g/L	15 g/L
NaH2PO2·H2O	8 g/L	8 g/L	8 g/L	8 g/L
Temperature	65	65	65	65
pH	9–9.5	9–9.5	9–9.5	9–9.5
Al2O3	–	10 g/L	–	2 g/L
GO	–	–	200 mg/L	200 mg/L

2.2. Characterization

The characterization steps were given in Fig. 2. The coating surface morphologies and chemical compositions were identified using Phillips XL30 Field Emission Scanning Electron Microscopy (FESEM) coupled energy-dispersive X-ray spectroscopy (EDS). The phase and structure of coatings were investigated by X-ray diffractometer (Rigaku RINT 2200, Japan) using Cu Kα radiation operated at 40 kV. Raman spectra were measured using Raman spectrometer. The crystallite size and micro-strain of the samples were estimated via the Williamson Hall equation according to the FWHM of all peaks of the coating [30–32]. The coating thickness was calculated from the cross-sectional by Field Emission Scanning Electron Microscopy. The coating surface roughness was measured using a surface profilometer. The amount of incorporating reinforcement in the coating was determined using image analysis by the energy-dispersive X-ray spectroscopy (EDS).

Nanohardness and elastic modulus of the coatings was determined from cross-section with an instrumental nanoindenter using a load of 100 mN and a time of 10 s with a Berkovich diamond indenter by applying the Oliver-Pharr analysis [33]. Five readings were taken at different places on each deposit and then the values were averaged. Tribological tests were carried out using a reciprocating type pin-on-disc tribometer (TRB model CSM Instruments device) at a load of 1 N with a sliding speed of 200 mm/s against M50 balls (62 HRC) with a diameter of 10 mm. The behavior of the coatings was examined during the wear tests and a single repetition was performed.To calculate the area of the worn coating was used surface profilometer (KLA Tencor P6). After tribological tests, wear tracks and wear mechanisms were analyzed by FESEM and SEM equipped with EDS. The wear rate was calculated by the volumetric loss [34].

The corrosion performance of the coatings was evaluated by potentiodynamic polarization curves and electrochemical impedance spectroscopy (EIS) at room temperature. Electrochemical tests were carried out using a classical three electrodes cell at the sodium chloride (NaCl) solution with saturated calomel electrode SCE (+0.242 V versus SHE) as the reference electrode, platinum as the counter electrode, and the coating with an exposed area of 1 cm^2 as a working electrode. The potentiodynamic polarization curves were performed using a GAMRY at a constant voltage scan rate of 0.3 mV/s. Electrochemical impedance spectroscopy (EIS) measurements were carried out using Reference 600

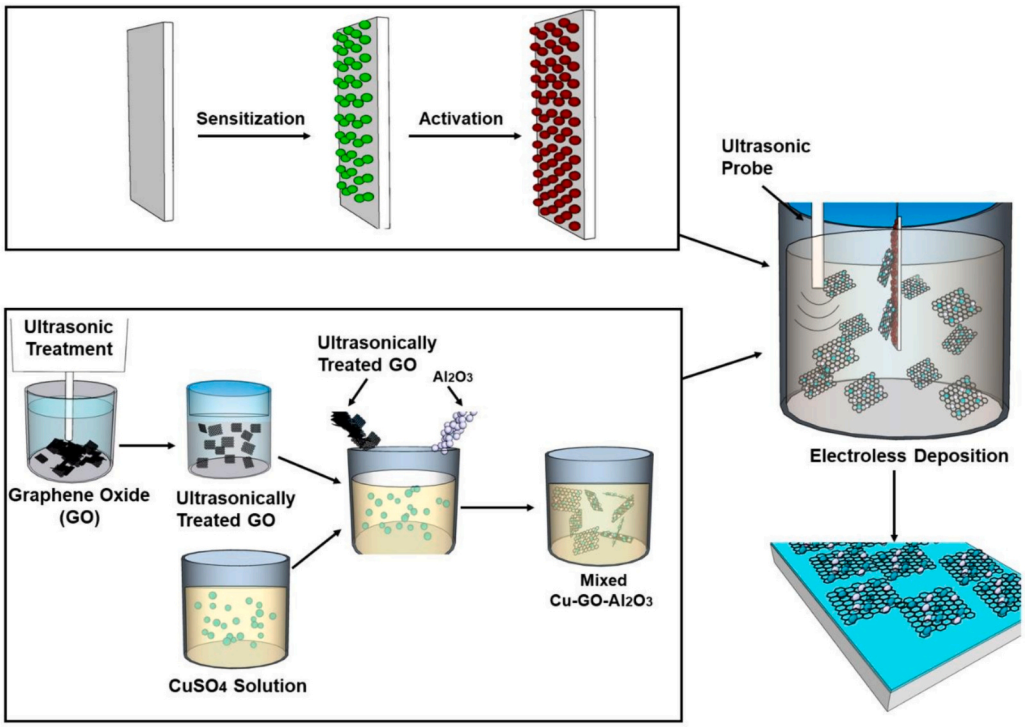

Fig. 1. Schematic of production of Cu-based composite coatings.

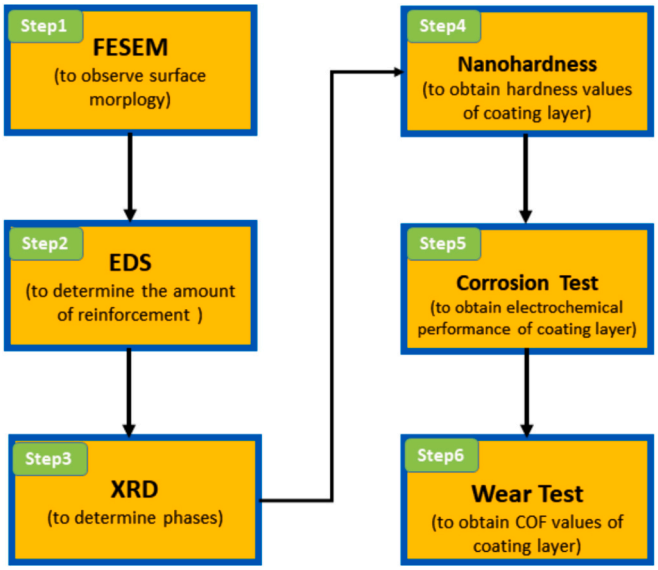

Fig. 2. Flow-chart of characterization of Cu-based composite coatings.

Gamry potentiostat within the frequency range from 100 kHz to 0.01 Hz with a low AC perturbation of 1 mV.

3. Results

The surface morphology of the pure Cu, Cu-Al2O3, Cu-GO, and Cu-GO-Al2O3 coatings has been investigated and displayed in Fig. 3. As noted, the surface of pure copper coating exhibits compact morphology with irregular pyramid-like shapes. The surface of the Cu-Al2O3 composite coating possesses a more compact and smoother surface morphology compared with a pure copper coating, as exhibited in Fig. 3a. The white dots are related to the Al2O3 ceramic particles incorporated in the copper matrix; Al2O3 particles are well dispersed with little agglomeration in the copper matrix. The dimensions of the ceramic particles range from 100 to 200 nm. On the other hand, it is undoubtedly understood that incorporating graphene oxide (GO) significantly affects the surface morphologies of copper composite coating (Fig. 3c-Fig. 3d). It can be observed that the substrate was well deposited and fully covered with copper without any surface cracks, which may be due to minimal interfacial strain at the interface of the coating and substrate for Cu-GO and Cu-GO-Al2O3 composite coating. Compared to Cu coating, the surface roughness of Cu-GO and Cu-GO-Al2O3 composite coating is reduced (Table 2). While calculating surface roughness values, more than one surface roughness was taken from the sample and the average roughness values were given with their standard deviations. The SEM images of the cross-section of the produced pure Cu, Cu-Al2O3, Cu-GO, Cu-GO-Al2O3 coatings are displayed in Supplementary Material Fig. S1. The thickness, incorporated Al2O3 and graphene oxide in the matrix are listed in Table 2. The additional contents (GO and Al_2O_3) were determined by EDS analysis. The surface morphology of Cu-GO-Al2O3 composite coating consists of fine spherical nodular, which indicates that the co-deposited graphene oxide and ceramic particles are uniformly distributed in the copper matrix. The composite coating became finer, and the compact structure was obtained when graphene oxide and Al2O3 particles were simultaneously incorporated into the copper matrix.

The higher magnification FESEM images of the Cu-GO and Cu-GO-Al_2O_3 composite coatings are shown in Fig. 4. As shown in Fig. 4a, the surface of the Cu-GO composite coating possesses a uniform and dense particular-like structure with a dimension of ~50–100 nm. It can be seen clearly that the graphene oxide is well incorporated into the copper coating and the co-deposited composite is growing as a network-like structure shown in the inset of Fig. 4a, as pointed out by the red dashes. On the other hand, the Cu-GO-Al_2O_3 composite coating structure is more compact and refined than the Cu-GO composite coating, as demonstrated in Fig. 4b. It can be seen in the inset of Fig. 4b that alumina oxide particles are decorated on the wrinkled surfaces of graphene oxide. Literature has reported [35,36] that fine wrinkles are signs of homogeneous distribution of graphene oxide, which is clearly seen in

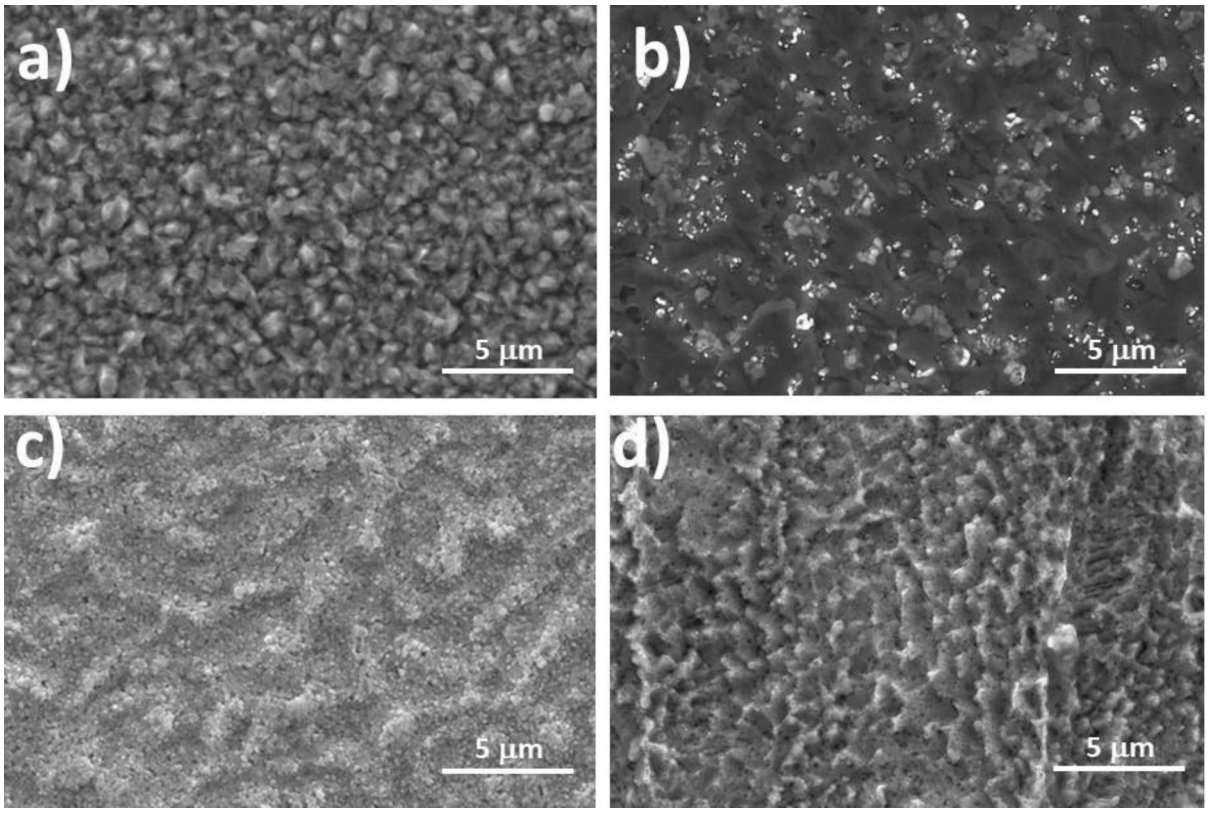

Fig. 3. FESEM images of (a) Cu, (b) Cu-Al_2O_3, (c) Cu-GO, and (d) Cu-GO-Al_2O_3coating.

Table 2
Thickness, surface roughness, incorporated Al_2O_3 content and incorporated GO content of the samples.

Coatings	Thickness (µm)	Surface roughness (µm) (Ra)	Incorporated Al2O3 content (wt%)	Incorporated GO content (wt%)
Cu	~24	140,11 ± 8.55	–	–
Cu-Al_2O_3	~25	125,25 ± 6.2	8.5	–
Cu-GO	~28	90,81 ± 1.25	–	7,2
Cu-GO-Al_2O_3	~30	105,83 ± 3.76	0,5	6,5

our study and the white dots are linked to the Al_2O_3 ceramic particles with a diameter of about 100–300 nm attached to the graphene oxide (inset in Fig. 4b). Al_2O_3 decorated with the graphene oxide was deposited as a cage network-like structure and uniformly anchored to the copper grains in the matrix under ultrasonic power, indicating that the coating is entirely dense. This may be attributed to the introduction of ultrasonic power, which reduces hydrogen absorption at the coatings, leading to a compact structure [37]. It is thought that graphene oxide decorated with Al_2O_3 significantly improves the nanomechanical, corrosion, and tribological properties of composite coating by acting as a spacer against the aggregation of individual graphene oxide.

Fig. 5 exhibits the element distribution maps of the Cu-GO- Al_2O_3 composite coating. This result confirms that the composite comprises Cu, C, Al, and O elements, and all the elements are evenly distributed. Additionally, the element distribution maps from cross-section of the Cu-GO- Al_2O_3 composite coating is shown in the Supplementary Material Fig. 2S. Besides the ultrasonic power, the reinforcement of graphene oxide was significant for the growth and nucleation of Cu-GO- Al_2O_3 coating. The Cu-GO- Al_2O_3 composite coating shows that new nucleation sites are formed when graphene oxide and ceramic particles are incorporated into the copper matrix. The reason might be the high growth rate of copper crystals and deposition rate with ultrasound conditions [38]. Under ultrasonic conditions, the graphene oxide dispersion and its amount in the copper matrix were improved. This may be due to acoustic streams that stem from ultrasonic power, which results in violent vibrations and high-pressure waves [39]. Another reason for improving the surface morphology of coating may be that microjets derived from ultrasonic cavitation energy could only be treated on the substrate [40]. Therefore, new nucleation sites appear on graphene oxide, forming an equiaxed cage network-like on the surface, which prevents the regular growth of the nodular grains.

The electroless coating consists of a redox reaction, which is the reduction of Cu^{2+} ions and the oxidation of hypophosphite ions [41]. A catalytic surface is required for electroless coating. Before electroless coating, the pre-treatment process is applied to the substrate materials to form the catalytic surface. Therefore, before coating, the substrate was sensitized by $SnCl_2$ solution, in which Sn^{+2} ions were adsorbed on the substrate to enhance the adsorption of palladium ions and then exposed to a solution containing Pd^{+} ions for activation. In this way, copper ions are easy to be deposited on the activated surfaces of the substrate. In the activation process, the palladium ions were reduced to the substrate, resulting in the reaction Sn^{2+} with the Pd^{2+} to form uniform Pd catalytic nuclei, leading to an easy reaction with copper ions on the substrate, as shown in Eq. (1) and Eq. (2) [42]. After electroless copper coating begins, the absorbed copper atoms will diffuse along the lateral surface of the substrate, then move to the proper nucleation sites, and at least the reduced Cu^{2+} ions were continuously deposited on the substrate (Eq. (3)). Graphene oxide and ceramic particles in the solution are transported to the substrate via ultrasonic stirring, and then when GO and Al_2O_3 arrive in the matrix, the copper subsequently traps them. Copper ions have reduction priority due to reduction potential, and the reduction reaction of graphene oxide occurred after Cu^{2+} was reduced to metallic copper. There are many defects and carboxylic groups at the edges of graphene oxide, resulting in a stronger interaction between

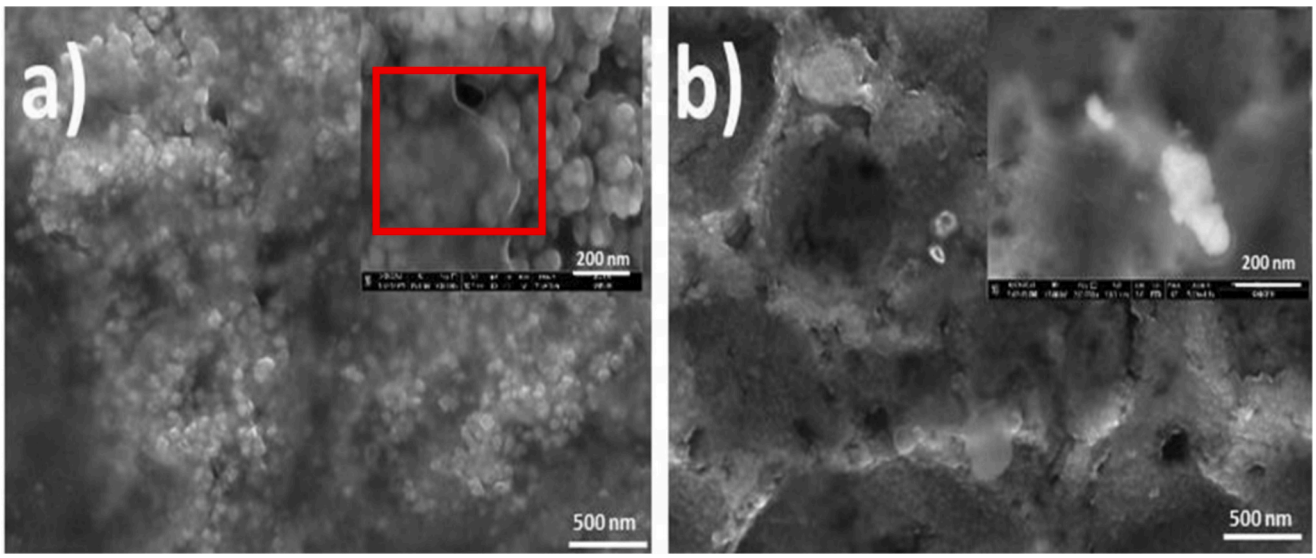

Fig. 4. High-magnification FESEM images of a) Cu-GO b) and Cu-GO-Al_2O_3 coating.

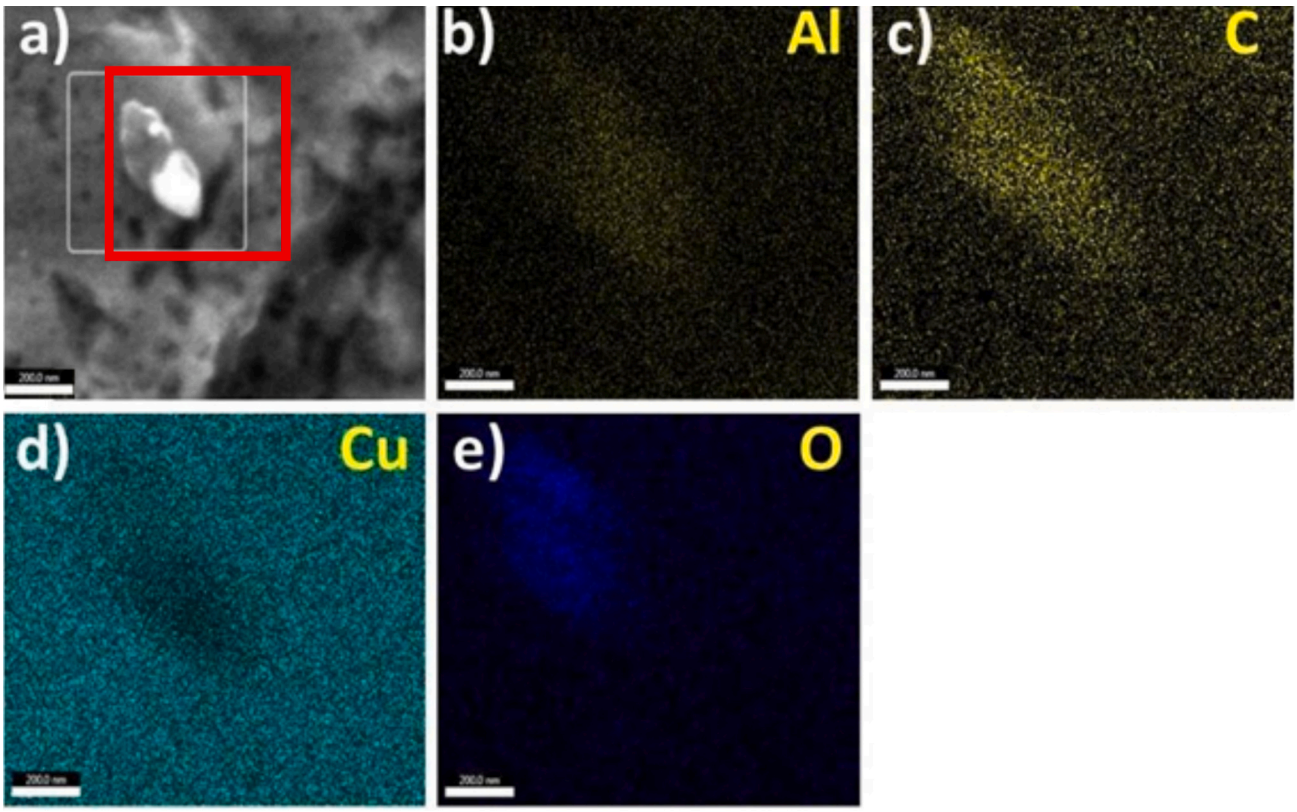

Fig. 5. Element distribution maps of Cu-GO-Al_2O_3 coating.

graphene oxide and copper and providing reaction sites for chemical bonding [43]. Therefore, the surface of graphene in the electrolyte was simultaneously reduced to copper from copper ions due to a defect in the graphene oxide, which enables more active sites for copper deposition. It can be seen that the Al_2O_3 particles decorated by graphene oxide existed at the surface with a typical wrapped structure, which oxide hydroxyl functional groups on the surface of graphene oxide and defect in the graphene oxide which led to the presence of additional nucleation sites for the copper deposition [43]. Moreover, GO acts as a catalyst surface, accelerating the reaction rate during electroless copper deposition. In other words, the growth rate in the surrounding area of GO and Al_2O_3 particles is slower than the nucleation rate of copper crystals. As a result, the introduction of GO and Al_2O_3 significantly refines the grains of the matrix. The surface morphology changes from the polyhedral pyramids to finer spherical–cage-like network structure, as shown in Fig. 6.

$$Pd^{2+} + Sn^{2+} \rightarrow Sn^{4+} + Pd^{0} \quad (1)$$

$$Pd + Cu^{2+} \rightarrow Pd^{2+} + Cu \quad (2)$$

$$Cu^{2+} + 2HCHO + 4OH^{-} \rightarrow Cu^{0} + 2HCOO^{-} + H_2O + 2H_2O \quad (3)$$

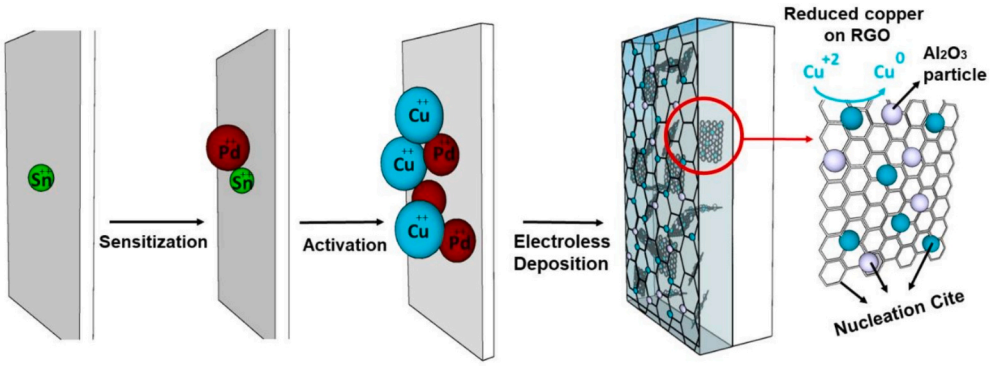

Fig. 6. Schematic of electroless composite coating mechanism of Cu-GO-Al_2O_3 coating.

Fig. 7a shows the XRD patterns of the Cu, Cu-Al_2O_3, Cu-GO, Cu-GO-Al_2O_3 coatings. As seen in Fig. 7a, all the coatings observed that the peaks at 43.31°, 50.44°, and 74.12°, belong to (111), (200), and (220) crystals with face-centered cubic (fcc) structures of copper, respectively (PDF No: 01–070–3038) [44,45]. The peak of the Al_2O_3 and graphene oxide were not noticed because the amount of graphene oxide and Al_2O_3 particles in the matrix was too small to measure. Furthermore, the effect of graphene oxide and Al_2O_3 particles on the micro-strain and crystallite size in the copper matrix was determined by using the Williamson-Hall method [33]. The average crystallite size of the copper matrix and micro-strain were calculated from XRD pattern and exhibited in Table 3. The functional groups such as carboxyl (COOH) and hydroxyl (OH) also provide nucleation sites for copper growth. The smallest crystallite size for Cu-GO-Al_2O_3 coating may be attributed to graphene oxide, and ceramics particles provide more nucleation sites for copper grains and retarded the grain growth of the copper matrix, which is due to a

Table 3
The average grain size and microstrain values of Cu grains crystallized in different orientations.

Coatings	Crystallite size (nm)	Microstrain
Cu	89	12.12×10^{-4}
Cu-Al_2O_3	75	23.22×10^{-4}
Cu-GO	42	63.59×10^{-4}
Cu-GO-Al_2O_3	29	$98{,}25 \times 10^{-4}$

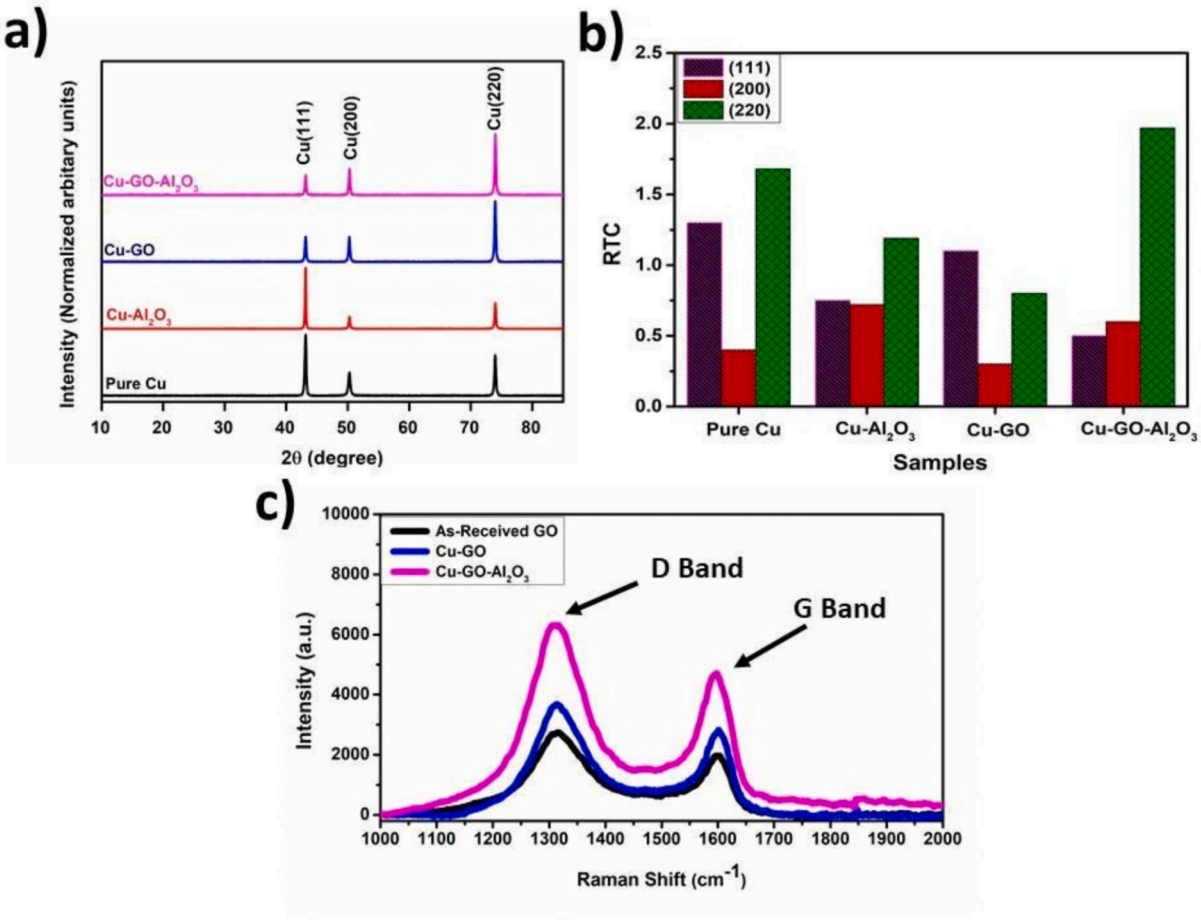

Fig. 7. (a) X-ray diffraction patterns (b) Texture orientation (c) Raman spectroscopy of Cu and Cu-Al_2O_3, Cu-GO, Cu-GO- Al_2O_3 coatings.

uniform distribution as network-like of graphene oxide in the matrix. Meanwhile, the micro-strain of the Cu-GO-Al_2O_3 coating was approximately 8.1 times higher than that of the pure copper coating. After incorporating the GO and Al_2O_3, the microstrain of the Cu-GO-Al_2O_3 coating increased. The diffraction peak intensity and texture of the copper coating were changed with the incorporation of graphene oxide and ceramic particles. The preferred orientation of copper coatings for the four major Cu peaks, (111), (200) and (220) was carried out with the texture coefficient (Tc) calculated by Eq. 4 [46]:

$$\boldsymbol{RTC} = \frac{Ihkl}{\Sigma Ihkl} x \frac{\Sigma I0hkl}{I0hkl} \tag{4}$$

where I (hkl) is the intensity of the hkl peak of the produced coatings, and I_0 (hkl) refers to a standard reference pattern. The relative texture coefficients of pure Cu, Cu- Al_2O_3, Cu-GO, Cu-GO- Al_2O_3 coatings are displayed in Fig. 6b. It is clearly seen from XRD analysis that the Cu phase crystallizes in different directions with the added Al_2O_3 and GO reinforcements. Relative texture coefficients (RTC) were calculated for pure Cu, Cu-Al_2O_3, Cu-GO and Cu-GO-Al_2O_3 coatings and are shown in Fig. 6b. Addition of Al_2O_3 and GO to the Cu matrix caused significant changes in the crystallographic orientations of the Cu phase. For pure Cu coating, the crystal growth orientations occurred mainly in the (111) and (200) planes. While the densities of the (200) and (220) planes decreased in Cu- Al_2O_3 coatings, the growth orientation of the Cu phase was in the (111) plane. Crystallization and growth of Cu grains in the (111) plane occurred as a result of grain boundary formation, which was affected by the microstructural interaction of Al_2O_3 reinforcement particles with the Cu matrix, and grain growth kinetics, which varied according to pure Cu coating. On the other hand, the addition of GO to the Cu matrix caused the growth to occur in a much different plane and the Cu grains preferred the (220) growth plane. This change is due to the stress distribution and grain boundary mobility that GO causes to change when it enters the structure during the coating process. In the Cu-GO- Al_2O_3 coating, where GO and Al_2O_3 are used together as reinforcement, the growth of Cu grains occurring in the (220) plane is more evident. Has been realised. The synergistic effect caused by GO and Al_2O_3 is an indication that there is an interaction between GO and Al_2O_3 particles. In addition, the dominance of Cu grain growth in the (220) plane in Cu-GO-Al_2O_3 coatings reveals that GO is the reinforcing particle that is effective in the grain growth mechanism.

Raman spectrum is extensively used to characterize crystallization defects and the structure of graphene-based composites. The Raman spectra of Cu-Al_2O_3, Cu-GO, Cu-GO- Al_2O_3 composite coatings, and original graphene oxide are shown in Fig. 7c. There are two characteristic peaks of the graphene oxide at 1330 cm^{-1} and 1590 cm^{-1}, which relate to carbonaceous materials D and G peaks, respectively [47]. G peak corresponds to the first-order scattering of E2g mode for sp^2 C—C double bond in graphene plane, while the D band is related to the presence of structural disorder in graphene due to epoxide and hydroxyl functional groups. From Fig. 7c, it is clear that D and G peaks were observed in the copper coatings, indicating graphene oxide was successfully added to the coating with electroless coating. The intensity ratio of D to G peak $I_{(D)}/I_{(G)}$ can also determine by Raman spectroscopy to characterize structural defects [48]. We can see that the ratios of $I_{(D)}/I_{(G)}$ are changed Cu-GO, Cu-GO-Al_2O_3 composite coatings compared with that of the original graphene oxide. The variations of $I_{(D)}/I_{(G)}$ in the defects of Cu-GO, Cu-GO- Al_2O_3 coatings are 0.74 and 0.77, respectively, increase compared to that in the original graphene oxide, indicating a higher density of the structural defects in Cu-GO- Al_2O_3 coating.

The elastic modulus and nano hardness of the pure Cu, Cu- Al_2O_3, Cu-GO, Cu-GO- Al_2O_3 coatings were characterized by nanoindenter by a Berkovich tip. Both load-depth and hardness-depth (Fig. 8a) curve evident that all composite coatings exhibited higher hardness than pure copper. It can be seen from Fig. 8b that compared with those of pure Cu samples, the nano hardness and elastic modulus values of Cu-GO coatings are 1.67 GPa and 272 GPa, which are improved by ~22,75 % and ~14,7 %, respectively. The elastic modulus of Cu-GO-Al2O3 coatings was found to be 340 GPa, which is ~1.5 times higher than that of the pure Cu coating. The nanohardness of Cu-GO-Al_2O_3 composites is increased to 3.4 GPa compared to those of Cu-GO composite coating, which is attributed to the excellent interfacial and synergetic strengthening of graphene oxide and Al_2O_3 particles. As a result, the Cu-GO-Al_2O_3 coating has a higher elastic modulus and nanohardness among all the coatings. The nanohardness and elastic modulus enhancement can be explained by several mechanisms such as load transfer, grain refinement, and Orowan looping [49–52]. The load transfer is an important mechanism in enhancing the nanomechanical properties of graphene-based copper coatings. It suggested that OH^- and $COOH^-$ functional groups on the graphene oxide can increase interaction with Cu^{2+} and occur chemical bonds between GO and Cu^{2+} ions, effectively transferring load from the Cu matrix to GO and improving the mechanical properties [52]. It was clear that graphene oxide was incorporated as a network structure like into the Cu matrix, and porosity was not observed in the coating surface, indicating a high interfacial strength due to strong interfacial bonding between the GO and metal matrix [53]. Therefore, the Cu matrix could effectively transfer the load from the Cu matrix to the graphene oxide under external force via shear stresses. As discussed, graphene oxide and Al_2O_3 are known to refine grain size during electroless coating because they act as nucleating sites for grain

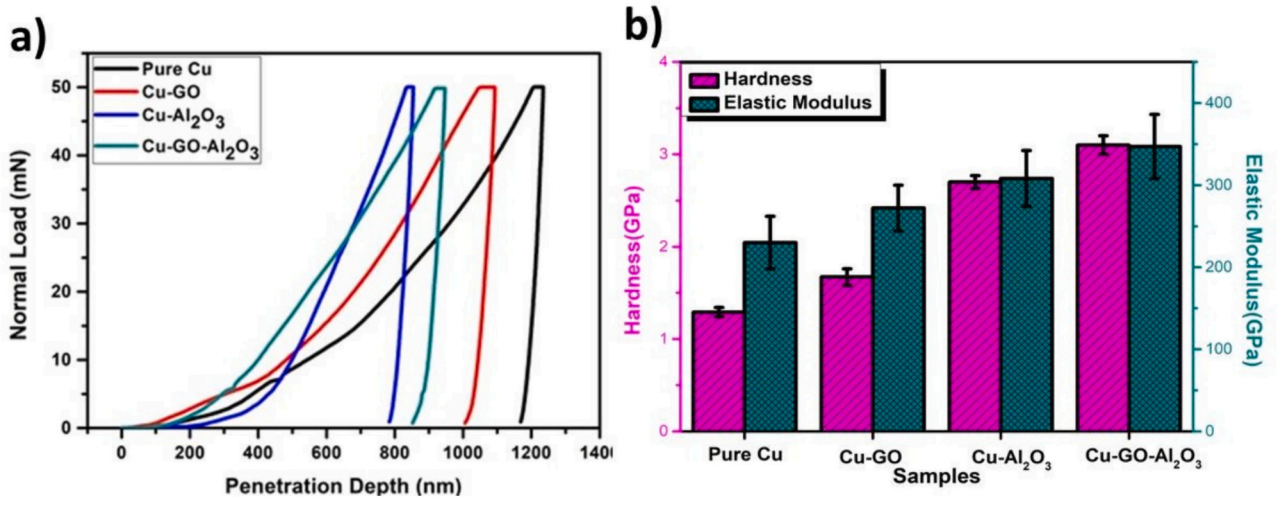

Fig. 8. a) typical load vs. depth curves b) The nanohardness and elastic modulus of pure Cu, Cu-Al_2O_3, Cu-GO, Cu-GO-Al_2O_3.

refinement. The graphene oxide and Al_2O_3 particles were uniformly distributed in the coating, and the grain size was reduced, which simultaneously increased the grain boundaries. Therefore, the graphene oxide and Al_2O_3 particles prevent the movement of the dislocations, resulting in the increase of dislocations and stress, which contribute to the improved mechanical properties of the coating. Additionally, refined copper grains via the pinning effect also played an important role in enhancing the nanomechanical properties of graphene-based copper coatings. The incorporation of ceramic particles and GO into the copper matrix led to a distortion of the copper lattice due to the formation of a compressive micro-strain.

Fig. 9 shows the friction coefficients and wear rate for pure Cu, Cu-Al2O3, Cu-GO, Cu-GO-Al_2O_3 under a 1 N load and 200 mm/s sliding speed. As shown in Fig. 9a, the coefficient of friction of all the composite coating displayed decreased compared to the pure copper coating. For the pure copper coating, the friction coefficient increased to a high value of approximately 0.6. As for Cu- Al_2O_3 coating, the friction coefficient fluctuated during all tests and remained at a value of roughly 0.4–0.5. It is also noticed that the friction coefficient of copper and Cu- Al_2O_3 composite coatings fluctuate much more intensely than that of graphene-based composite coating. This fluctuation of friction coefficient may be attributed to repeated localized adhesion of worn debris and the breakdown of the adhered wear debris. It can be seen from Fig. 9a that the friction coefficient of the Cu-GO- Al_2O_3 composite coating is around 0.17, which is much smaller than 0.6 for pure copper coating and 0.45 for Cu-Al_2O_3. The reduced friction coefficient may be due to Al_2O_3 decorated graphene oxide can serve as spacers reducing shear force, which hinders the rough contact between coating and ball. (decrease the metal-to-metal contact) [53]. Another reason for friction coefficient is the combined effect of Al_2O_3 and graphene oxide, which provides a self-lubricating impact on the copper matrix in a reduced coefficient of friction. This result is in very good agreement with the other researcher [54,55]. The friction coefficients of Cu-GO-Al_2O_3 composite coating more smoothly than that of Cu-GO composite coating, indicating that incorporating graphene oxide and ceramic particles into the metal matrix is beneficial to tribological properties. During the tests, the wear rate of the pure copper, Cu-Al_2O_3, Cu-GO, Cu-GO-Al_2O_3 is summarized in Fig. 9b. The unreinforced Cu deposition copper coating shows the highest wear rate with the range of 4.2×10–5 mm^3/Nm This indicates that unreinforced Cu deposition is subject to severe damage during the sliding wear test. Compared with the pure copper coating, the wear rate for Cu-Al_2O_3, Cu-GO, Cu-GO-Al_2O_3 were reduced by 10.1 %, 35.6 %, and 57.6 %, respectively.

Fig. 10 displays the morphology of the worn pure copper, Cu-Al_2O_3, Cu-GO, Cu-GO- Al_2O_3. From Fig. 10a, it is clearly seen that the severe plastic deformation of the pure copper due to the high adhesion between the counterball and the pure Cu, followed by the flowing of wear products to the worn surface. Due to the plastic deformation hardening of copper and the wear products deposited on the worn surface, very finely dispersed delamination products are observed on the surface. Adhesive wear is considered to be the dominant wear mechanism for pure copper and this wear mechanism is in consistent with its higher wear rate [56]. The FESEM image in Fig. 10b shows the plastic deformation of the Cu matrix again, but the intensity of the adhesion effect has been decreased together with some abrasive grooves, and a few wear debris for Cu-Al_2O_3 composite coating. It can be concluded that the predominant wear mechanism is again adhesive for Cu- Al_2O_3 coating. In the case of the Cu-GO composite coating, the appearance of the worn surface is relatively smooth with only a few microploughs microcracks observations. It has been evaluated that, because of the improved load-bearing effect of the GO reinforcements and the lubrication contribution, both the adhesion and the abrasion are decreased on the worn surface as the grooves reveal fine scratches on the worn surface. The microcracks are evaluated as evidence that the thin layer of plastic deformation results in fatigue crack generation and expectation of delamination wear mechanisms by joining the lateral fatigue cracks beneath the surface. On the contrary, the worn surface of Cu-GO- Al_2O_3 composite coating shows that the deep grooves disappear and are observed to be smoother worn without any obvious microcrack. The grooves become fine and shallow compared with Cu-GO composite coating (Fig. 10c-d). Reinforcing the Cu matrix with GO- Al_2O_3 decreases the adhesion and abrasion effects since the load-bearing capability can improve the tribological behavior. In this hybrid composite deposition condition, Al_2O_3 reinforcement contributed mainly to the load-bearing ability and improved the surface sensitivity of the Cu matrix, and GO mainly friction for the matrix. Therefore, after incorporating ceramic particles and graphene oxide into the Cu matrix, the crack caused by fatigue and resultant delamination has been eliminated. It is concluded that reinforcing the Cu matrix with GO and Al_2O_3 in the form of hybrid composite results in effectively restraining plastic deformation, successfully bearing the load. These results indicate the main wear mechanism of Cu-GO- Al_2O_3 composite coating is a mixed type of mild abrasive and adhesive wear with prevented delamination risks. The formation of a graphene-rich transfer film at the top of the wear path is only possible with a sufficient amount of uniformly dispersed graphene oxide in the matrix. We concluded that the low content and only graphene oxide reinforcements could not play a favorable self-lubricating role in Cu composite coating. The distribution of the ceramic particle decorated graphene oxide at the interface of the mating surface not just inhibits the copper from being oxidized but also improves wear performance due to the low shear strength of GO. The wear scar diameters of counterball of pure copper coating and Cu-GO-Al_2O_3 composite coating is shown in Fig. 10e and Fig. 10f. It can be seen from Fig. 10e-f that the wear scar formed on counterball for pure copper

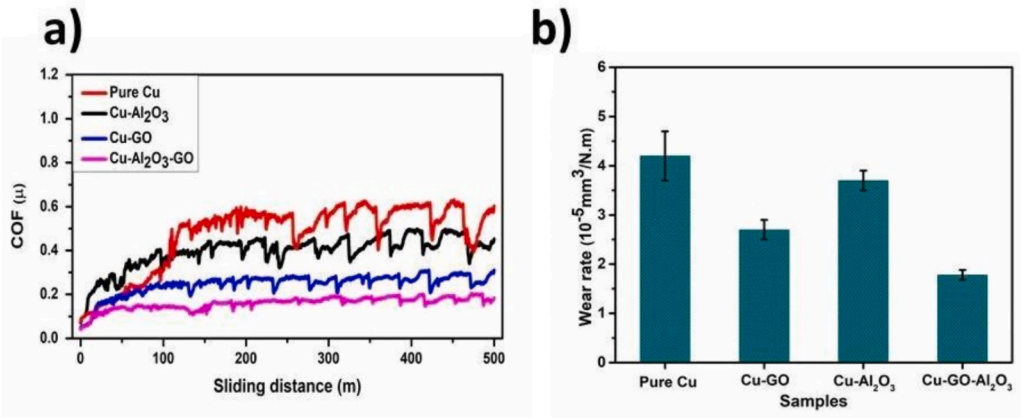

Fig. 9. Wear test results of samples: a) friction coefficients b) wear rate.

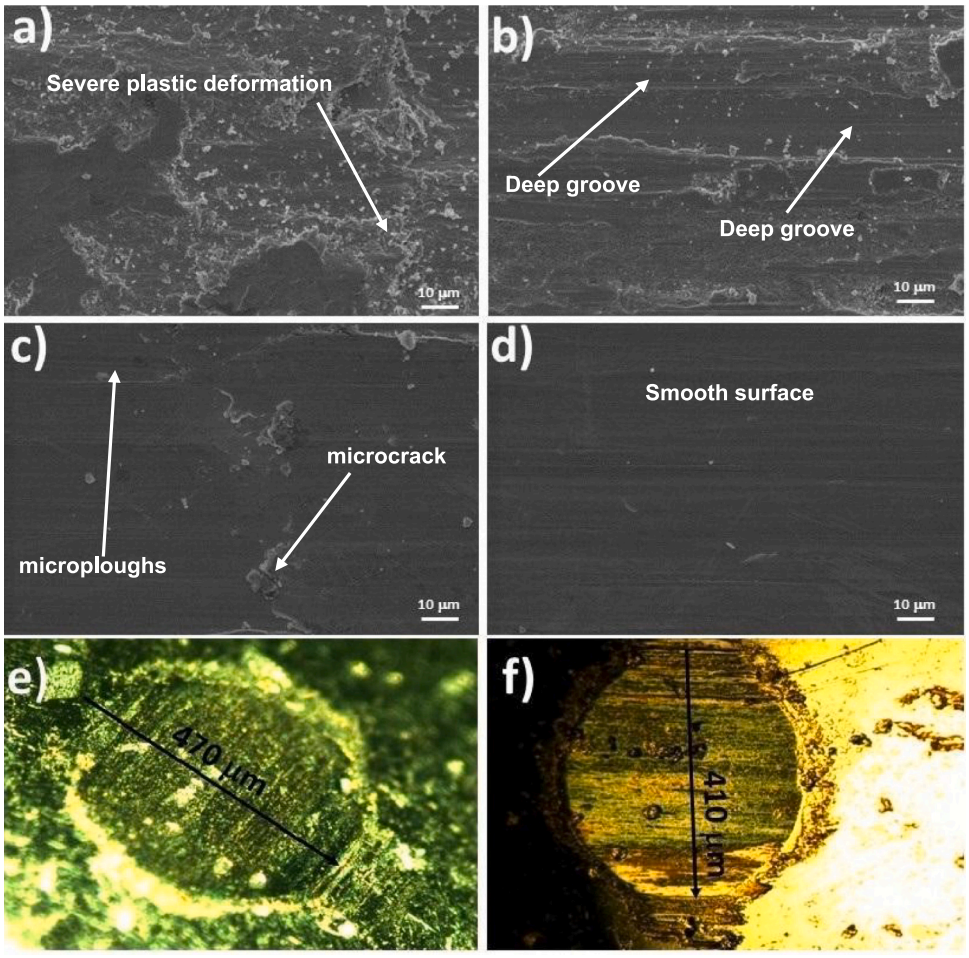

Fig. 10. SEM image of the worn surface of a) Cu b) Cu-Al_2O_3 c) Cu-GO d) Cu-GO- Al_2O_3 composite coating e) wear track of counterball after sliding against copper coating f) wear track of counterball after sliding against Cu-GO- Al_2O_3.

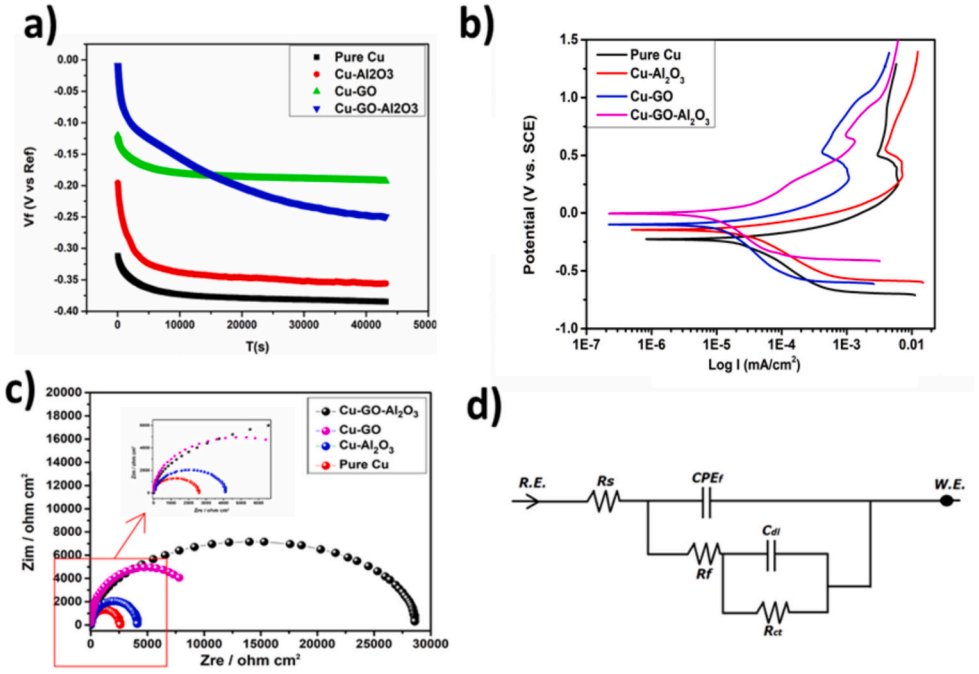

Fig. 11. Electrochemical results of the coatings tested in 3.5 wt% NaCl: a) open circuit potential (OCP) change b) Tafel curves c) Nyquist plots d) Equivalent circuit model used to analyze the EIS data.

is significantly larger than that of Cu-GO-Al_2O_3 composite coating. The wear scar diameters of counterball of pure copper coating and Cu-GO-Al_2O_3 composite coating were 470 μm and 410 μm, respectively. It has been observed that wear debris consisting of copper and oxides were transferred and adhered to the surface of the counterball, which indicates severe wear takes place during the sliding test for pure copper coating (Fig. 10e). The wear track of counterball seemed to be uniform and smooth, with no large debris particles, which indicated slight wear of the counterpart(Fig. 10f).

To investigate the electrochemical behaviors of all samples, Tafel polarization studies were performed using 3.5 % NaCl. Fig. 11a exhibits the open circuit potential (OCP) change vs. time for pure copper, Cu-Al2O3, Cu-GO, Cu-GO- Al_2O_3 composite coatings in 3.5 % NaCl solution. Among all samples, Cu-GO- Al_2O_3 composite coatings, the OCP has more positive values. Fig. 11b shows the potentiodynamic polarization curves of the pure copper, Cu-Al_2O_3, Cu-GO, Cu-GO-Al_2O_3 composite coatings. Table 4 are listed the electrochemical kinetic data determined from the Tafel curves. The Tafel curves show that the corrosion potential is −0.381 V, −0.213 V, −0.139 V and −0.027 V for pure copper, Cu-Al_2O_3, Cu-GO, Cu-GO- Al_2O_3 composite coatings, respectively. In addition, the corrosion current density (icorr) values of the pure copper, Cu-Al_2O_3, Cu-GO, Cu-GO- Al_2O_3 composite coatings were 4.99×10^{-5}, 4.505×10^{-5}, 1.819×10^{-5}, and 9.9×10^{-6} μA·cm^{-2}, respectively. Compared to the pure Cu coating, the composite coatings displayed higher positive corrosion potentials and lower corrosion current densities, indicating that ceramic particles and graphene oxide significantly enhanced the corrosion resistance of the copper matrix. Notably, among all composite coatings, the Cu-GO-Al_2O_3 composite coatings displayed the lowest corrosion current densities and higher positive corrosion potentials value of 9.9×10^{-6} μA·cm^{-2} and −0.0275 V, respectively. This may be attributed to the coating suppressing both the anodic and cathodic reactions because the graphene and ceramic particles form an intense protective layer that enhances the electrochemical properties of the Cu matrix even in a very aggressive Cl^- environment [57]. The corrosion rate was calculated by Faraday law with ASTM Standard G10247 using the following Eq. (5) [58]:

$$\textit{Corrosion Rate} = Kx\frac{Icorr}{\rho A}x\frac{M}{Z} \quad (5)$$

where, K is the corrosion rate constant, 3272 mm year^{-1}; ρ is the density of copper; and A is the coating surface area, M is the molar mass of the copper (58.69 g mol^{-1}); z is the electron number. The corrosion rate calculation shows that the pure copper, Cu-Al_2O_3, Cu-GO, Cu-GO- Al_2O_3 composite coatings were 0.409, 0.369, 0.149, and 0.081 mpy, respectively. Cu-GO- Al_2O_3 composite coatings possessed the highest corrosion resistance. For the Cu-GO- Al_2O_3 composite coatings, the improved corrosion resistance may be attributed to the compact structure and refined grains due to the ceramic particles and the high impermeability of graphene oxide, which act as corrosion protection barriers to block the copper ion diffusion over the matrix.

Electrochemical impedance spectroscopy (EIS) was used to determine the corrosion resistance of the coatings. Electrochemical impedance results of the samples are exhibited in Fig. 11c. Fig. 11d is related to the equivalent circuit of the composite coatings and the resulting data in Table 5. In Table 5, the Rc, Rct, Rs, CPE, and Cdl represented the graphene coating resistance, charge transfer resistance, solution resistance, capacitance of coating, and double-layer capacitance, respectively. The real impedance of the pure copper is much smaller than that of all composite coatings. The incorporation of the ceramic particle and graphene oxide has significantly enhanced the radius of the impedance of composite coatings. The composite coating prepared with Al2O3 decorated graphene oxide has the largest radius of impedance semicircle, indicating higher the corrosion resistance for Cu-GO-Al2O3 composite coating. Al2O3 decorated graphene oxide in the matrix has increased charge transfer resistance (Rct) while CPE of electric double- layer capacitance (CPEdl) has reduced. This may be due to structural modification in the coating by the simultaneous addition of Al2O3 and graphene oxide reinforcements into the matrix. The Al2O3 decorated graphene oxide has served as a good barrier to inhibit the electrolyte invading the coating and decreases the structural and surface defects by filling micron holes and gaps in the copper matrix.

Table 4
Corrosion current densities, corrosion potentials and corrosion rate of samples.

Samples	Ecorr (V vs. SCE)	Icorr (μA·cm^{-2})	Corrosion rate (×10^{-2} mm year^{-1})
Pure Copper	−0.311	4.99×10^{-5}	0.409
Cu-Al_2O_3	−0.213	4.505×10^{-5}	0.369
Cu-GO	−0.139	1.819×10^{-5}	0.149
Cu-GO-Al_2O_3	−0.0275	9.9×10^{-6}	0.081

Table 5
Electrochemical impedance spectroscopy data of the samples by fitting.

Samples	Rs (Ω·cm^2)	CPE (10^{-7} F·cm^{-2})	Rf (Ω·cm^2)	Rct (Ω·cm^2)	Cdl (μF)
Pure Copper	20.85	94.78	1.2×10^4	28.17	2.58×10^{-4}
Cu-Al_2O_3	49.57	87.45	1.31×10^4	32.45	9.7×10^{-4}
Cu-GO	53.63	79.36	1.38×10^4	39.17	2.82×10^{-5}
Cu-GO-Al_2O_3	91.58	62.66	1.45×10^4	49.75	1.68×10^{-7}

4. Discussion

It is no doubt that the copper-based composite materials for the application of nano-devices or electrical contact materials have excellent corrosion and friction properties. The reasons for the enhancement of tribology performance can be attributed to several mechanisms; (i) grain refinement-hardness, (ii) self-lubricant layer, (iii) formation nanorolling. Firstly, the grain refinement in the copper coating leads to decreasing plasticity and increasing hardness, improving wear resistance. Moreover, the enhancement of friction and wear for the Cu-GO-Al_2O_3 composite coating can be due directly to the increase in nanohardness of the Cu-GO- Al_2O_3 coating by incorporating graphene oxide and Al_2O_3 particles and agrees with Archard's theory. According to Archard's theory [56], in which the wear rate of a material is inversely proportional to its hardness, the increased hardness can improve the tribology properties of the coatings. In this paper, incorporating graphene oxide and ceramic particles can improve the load-carrying capacity of carbon-rich self-lubricant film layer because it can act as a low shear strength film that effectively reduces the friction coefficient and wear rate.

Finally, The Al_2O_3 decorated graphene oxide nanorolls observed on the wear track could be the key to the significant decline of the COF and excellent wear performance because they serve as a roller bearing-like effect [25,59–61]. This prompted us to use Al_2O_3 particles, which may serve as nanoroll bearings when decorated on graphene, promoting superior mechanical resistance. Several studies have reported that ceramic nanoparticles such as Al_2O_3 and SiO_2 might form nanorolls between the mating surfaces during the wear test, especially in water vapor-containing environments [61]. These nanoscrolls could decrease metal-to-metal contact and change from the sliding friction to the rolling- sliding friction mixture thus improving the tribological performance. Graphene nanoscrolls were observed on the surface of the carbonous layer during the wear test, leading to superb friction-reducing. Llorente et al. [62] reported the formation of graphene nanoscrolls from graphene-based composite materials. As seen in Fig. 12a, graphene oxides are incorporated into the copper surface parallel to the sliding direction. When graphene oxide is subject to the

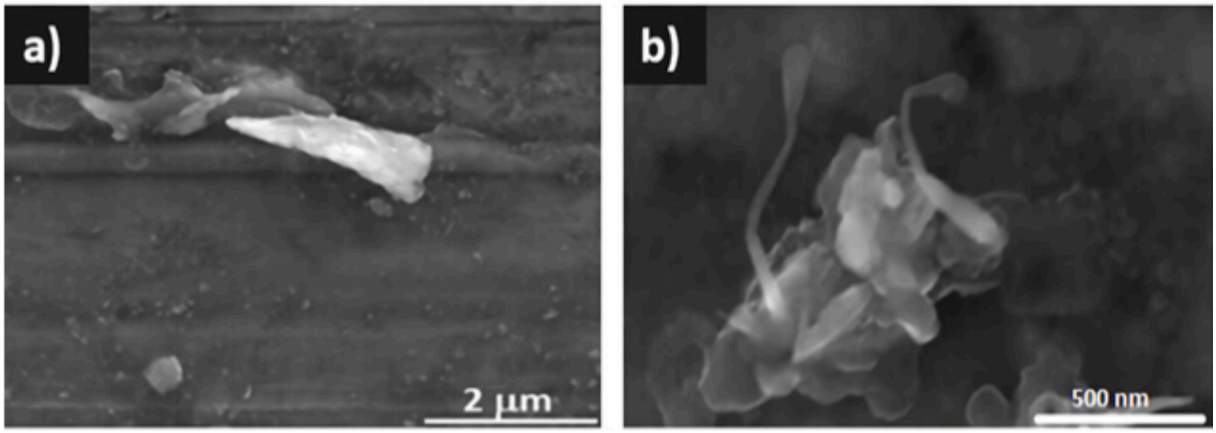

Fig. 12. High magnification FESEM micrograph showing formation nanorolls on top of the Cu-GO- Al_2O_3 composite coating a) 5000× b) 20,000×.

ball during the wear process, the graphene slide over others because of the shear forces. Some graphene oxides are peeled off by the slider, producing carbonaceous debris caused to roll up to form a nanoscroll structure with graphene crumpled around ceramic particles that would enhance the bearing capability. In our present work, nanoscrolls were observed existing within the worn surface in dry conditions, as shown in Fig. 12b. As shown in Fig. 12b, the graphene oxide nanorolls were observed perpendicular to the sliding direction at closing the edges of the worn surface and region with high contact pressure. We have observed the formation of graphene nanorolls, for Cu-GO- Al_2O_3 composite coating. In the literature, the formation of nanorolls during the wear of graphene based composite materials has been described. However, to the best of our knowledge, this is the first time that the formation of this kind of nanoroll in Al_2O_3 decorated graphene oxide coating has been reported. Thus, we have shown that the synergies of Al_2O_3 decorated graphene oxide incorporated in the copper matrix can significantly improve the tribological performances compared with those of other composite coatings.

In seawater conditions, it is generally accepted that the passivation layer consisting of ($Cu_2(OH)_3Cl$) or Cu_2O can be formed on the copper surface [2]. The smaller crystallite size can further induce its formation. The low hydrogen overvoltage on the Cu-GO-Al_2O_3 composite coating increases preferred copper dissolution and facilitates passive layer formation due to the incorporation of graphene oxide and ceramic particles. At the coating surface or the coating/solution interface, this passive layer prevents the dissolution of copper atoms and protects Cu from further corrosion as Cu ions. What's more, the addition of GO and ceramic particles can significantly refine the microstructure of coating, as the discussion above. The compact and without defects of surface morphology and finer microstructure for Cu-GO-Al_2O_3 coating reduces the active contact at the coating/solution interface against corrosion due to the uniformly distributed corrosion current, which may lead to enhancing the corrosion resistance. Another major factor in the improvement of electrochemical performance of Cu-GO-Al_2O_3 composite coating may be related to forming a network structure and low chemical reactivity of the ceramic particle decorated graphene oxide at the coating/electrolyte interface, which can act as a physical barrier to molecules such as H_2O and Cl^- ions transport at the coating/solution interface. Additionally, the surface morphologies of the pure copper coating and Cu-GO-Al_2O_3 after electrochemical corrosion test is shown in the Supplementary Material Fig. 3S.

Furthermore, the uniform distribution of the graphene oxide and ceramic particles may contribute to the improved corrosion resistance due to inhibiting localized corrosion. Our study obtained the outstanding comprehensive properties of Cu composite coating by incorporating Al_2O_3 particles and graphene oxide. As seen in Fig. 13, the Cu-GO- Al_2O_3 coating in our research is superior to most of those graphene-based copper composite coating in terms of electrochemical,

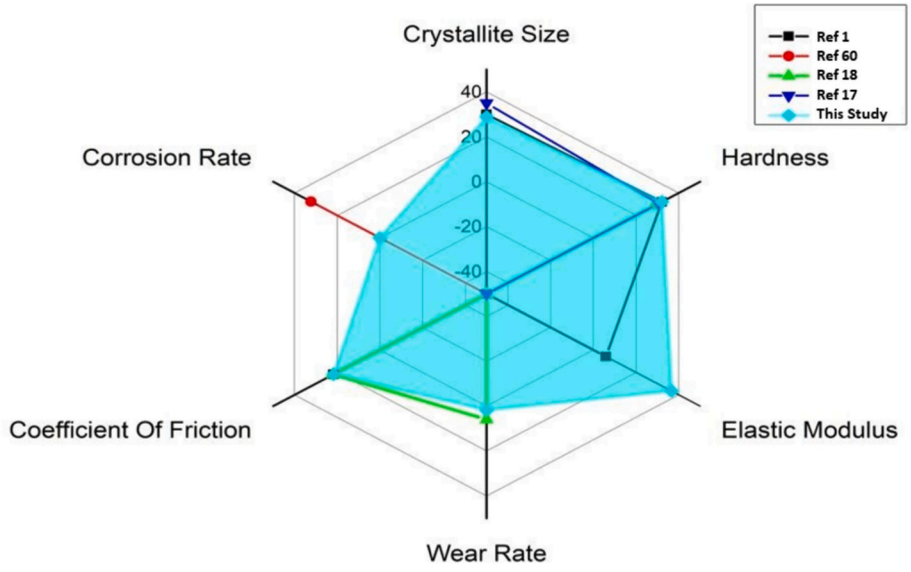

Fig. 13. The comparison of this study with the other studies in literature in terms of electrochemical, friction, wear rate and nanomechanical properties.

friction, wear rate and nanomechanical properties compared with the previous study [1,17,18,62].

In addition, Zhan et al. [63] added GO and CNT to the Cu matrix and observed quite good increases in corrosion resistance. They reported that this resistance was much higher as a result of the joint reinforcement of GO and CNT and suggested that this was due to the synergistic effect of GO and CNT. When the results they obtained were compared with this study, the corrosion resistance was lower. In another study, Cu-GO electro-composite coating was applied on pure Cu foil and it was observed that the hardness value was almost doubled [64].

5. Conclusions

In summary, the finer particulate- spherical -like network structure of Cu-GO- Al_2O_3 coating was successfully prepared via ultrasonic assisted electroless coating method.

- The composite coating reinforced with GO and Al_2O_3 particles delivered a lattice strain of 98,25 $\times 10^{-4}$, a crystallite size of 42 nm, a high nanohardness of 3,4 GPa and a high elastic modulus of 340 GPa, which are about 56 % and 62 % higher than those of the copper coating, respectively.
- It was found that the incorporation of GO and ceramic particles to improve the friction and wear rate of copper matrix can significantly improve the friction and wear rate of the copper matrix by decreasing the adhesion between coating and counterball and encouraging the stability of oxide tribo-film on the wear track. It is believed that the synergistic effect of GO and ceramic particles led to formation of graphene nanorolls in tribofilms, suggesting an additional lubricating effect.
- The electrochemical studies in 3.5 wt% NaCl solution displayed that Cu-GO-Al_2O_3 coating has good corrosion resistance than pure Cu coating due to the barrier property of GO and inert ceramic particles. It is suggested that the formation spherical-like network structure is crucial for achieving extraordinary performance.
- The ultrasonic-assisted electroless coating process has advantages, such as easy and simple operation, excellent performance, and is suitable for industrial manufacture. The Cu-GO-Al_2O_3 coating is expected to be used in next-generation electric contact and nano-electromechanical systems (NEMS) due to its excellent tribological, corrosion and nanomechanical properties.

CRediT authorship contribution statement

Sezer Tan: Methodology, Investigation. **Melisa Köse:** Writing – review & editing, Investigation. **Hasan Algül:** Resources, Investigation. **Mert Aydin:** Writing – original draft, Methodology. **Miraç Alaf:** Writing – review & editing, Resources. **Ahmet Alp:** Methodology, Investigation. **Hatem Akbulut:** Writing – review & editing, Writing – original draft. **Mehmet Uysal:** Writing – review & editing, Writing – original draft, Supervision.

Declaration of competing interest

The authors declare that they have no known competing financial interests or personal relationships that could have appeared to influence the work reported in this paper.

Data availability

No data was used for the research described in the article.

Appendix A. Supplementary data

Supplementary data to this article can be found online at https://doi.org/10.1016/j.diamond.2024.111537.

References

[1] T. Wang, R. Zhao, K. Zhan, L. Bao, Y. Zhang, Z. Yang, Y. Yan, B. Zhao, J. Yang, Preparation of electro-reduced graphene oxide/copper composite foils with simultaneously enhanced thermal and mechanical properties by DC electro-deposition method, Mater. Sci. Eng. A 805 (2021) 140574, https://doi.org/10.1016/j.msea.2020.140574.

[2] S. Li, G. Song, Q. Fu, C. Pan, Preparation of cu- graphene coating via electroless plating for high mechanical property and corrosive resistance, J. Alloys Compd. 777 (2019) 877–885, https://doi.org/10.1016/j.jallcom.2018.11.031.

[3] G. Yang, R. Wang, D. Fang, T. Hu, C. Bao, J. Yi, Nano-silver modified carbon nanotubes to reinforce the copper matrix composites and their mechanical properties, Adv. Powder Technol. 33 (2022), https://doi.org/10.1016/j.apt.2022.103672.

[4] P. Wang, L. Wang, K. Kang, J. Yin, X. Xiong, H. Zhang, Microstructural, mechanical and tribological performances of carbon fiber reinforced copper/carbon composites, Compos. Part A Appl. Sci. Manuf. 142 (2021) 106247, https://doi.org/10.1016/j.compositesa.2020.106247.

[5] S.P. Dwivedi, A. Saxena, S. Sharma, G. Singh, J. Singh, M. Mia, S. Chattopadhyaya, A. Pramanik, D.Y. Pimenov, S. Wojciechowski, Effect of ball-milling process parameters on mechanical properties of Al/Al2O3/collagen powder composite using statistical approach, J. Mater. Res. Technol. 15 (2021) 2918–2932, https://doi.org/10.1016/j.jmrt.2021.09.082.

[6] R. Kumar, J. Singh, S. Sharma, C. Li, G. Królczyk, S. Wojciechowski, Neutrosophic entropy-based ingenious measurement for fast Fourier transforms based classification of process-parameters and wear resistance of friction-stir processed hybrid AA7075- B4C aluminium metal-matrix composites, J. Mater. Res. Technol. 20 (2022) 720–739, https://doi.org/10.1016/j.jmrt.2022.07.026.

[7] H. Rangaswamy, M.P. Gowdru Chandrashekarappa, D.Y. Pimenov, K. Giasin, S. Wojciechowski, Experimental investigation and optimization of compression moulding parameters for MWCNT/glass/Kevlar/epoxy composites on mechanical and tribological properties, J. Mater. Res. Technol. 15 (2021) 327–341, https://doi.org/10.1016/j.jmrt.2021.08.037.

[8] Y.S. Huang, X.T. Zeng, X.F. Hu, F.M. Liu, Corrosion resistance properties of electroless nickel composite coatings, Electrochim. Acta 49 (2004) 4313–4319, https://doi.org/10.1016/j.electacta.2004.04.023.

[9] J.N. Balaraju, T.S.N. Sankara Narayanan, S.K. Seshadri, Structure and phase transformation behaviour of electroless Ni-P composite coatings, Mater. Res. Bull. 41 (2006) 847–860, https://doi.org/10.1016/j.materresbull.2005.09.024.

[10] T. Zhimeng, W. Zemin, X. Lei, Z. Libo, H. Zhaohui, L. Jianhua, Thermal and tribological properties of MoS2 doped graphite/copper composites by microwave sintering, J. Mater. Res. Technol. 15 (2021) 6001–6010, https://doi.org/10.1016/j.jmrt.2021.11.053.

[11] F. Chen, Q.S. Mei, J.Y. Li, C.L. Li, L. Wan, G.D. Zhang, X.M. Mei, Z.H. Chen, T. Xu, Y.C. Wang, Fabrication of graphene/copper nanocomposites via in-situ delamination of graphite in copper by accumulative roll-compositing, Compos. Part B Eng. 216 (2021), https://doi.org/10.1016/j.compositesb.2021.108850.

[12] A. Joseph, B. Kirubasankar, A.M. Mathew, M. Narayanasamy, C. Yan, S. Angaiah, Influence of pulse reverse current parameters on electrodeposition of copper-graphene nanocomposite coating, Appl. Surf. Sci. Adv. 5 (2021) 100116, https://doi.org/10.1016/j.apsadv.2021.100116.

[13] L. Han, J. Wang, Y. Chen, Y. Huang, Y. Liu, Z. Wang, Fabrication and mechanical properties of WC nanoparticle dispersion-strengthened copper, Mater. Sci. Eng. A 817 (2021) 141274, https://doi.org/10.1016/j.msea.2021.141274.

[14] V.B. Mohan, K. Tak Lau, D. Hui, D. Bhattacharyya, Graphene-based materials and their composites: a review on production, applications and product limitations, Compos. Part B Eng. 142 (2018) 200–220, https://doi.org/10.1016/j.compositesb.2018.01.013.

[15] Y. Raghupathy, A. Kamboj, M.Y. Rekha, N.P. Narasimha Rao, C. Srivastava, Copper- graphene oxide composite coatings for corrosion protection of mild steel in 3.5% NaCl, Thin Solid Films 636 (2017) 107–115, https://doi.org/10.1016/j.tsf.2017.05.042.

[16] F. Chen, J. Ying, Y. Wang, S. Du, Z. Liu, Q. Huang, Effects of graphene content on the microstructure and properties of copper matrix composites, Carbon N. Y. 96 (2016) 836–842, https://doi.org/10.1016/j.carbon.2015.10.023.

[17] Q. Zhang, Z. Qin, Q. Luo, Z. Wu, L. Liu, B. Shen, W. Hu, Microstructure and nanoindentation behavior of cu composites reinforced with graphene nanoplatelets by electroless composite coating technique, Sci. Rep. 7 (2017) 1–12, https://doi.org/10.1038/s41598-017-01439-3.

[18] Y.J. Mai, M.P. Zhou, H.J. Ling, F.X. Chen, W.Q. Lian, X.H. Jie, Surfactant-free electrodeposition of reduced graphene oxide/copper composite coatings with enhanced wear resistance, Appl. Surf. Sci. 433 (2018) 232–239, https://doi.org/10.1016/j.apsusc.2017.10.014.

[19] B. Jin, D.B. Xiong, Z. Tan, G. Fan, Q. Guo, Y. Su, Z. Li, D. Zhang, Enhanced corrosion resistance in metal matrix composites assembled from graphene encapsulated copper nanoflakes, Carbon N. Y. 142 (2019) 482–490, https://doi.org/10.1016/j.carbon.2018.10.088.

[20] S. Şap, M. Uzun, Ü.A. Usca, D.Y. Pimenov, K. Giasin, S. Wojciechowski, Investigation on microstructure, mechanical, and tribological performance of Cu base hybrid composite materials, J. Mater. Res. Technol. 15 (2021) 6990–7003, https://doi.org/10.1016/j.jmrt.2021.11.114.

[21] A. Miranda-López, C.A. León-Patiño, E.A. Aguilar-Reyes, E. Bedolla-Becerril, G. Rodriguez-Ortiz, Effect of graphite addition on wear behaviour of hybrid Cu/TiC-Gr infiltrated composites, Wear 484–485 (2021), https://doi.org/10.1016/j.wear.2021.203793.

[22] X. Chen, R. Bao, J. Yi, D. Fang, J. Tao, F. Li, Enhancing mechanical properties of pure copper-based materials with CrxOy nanoparticles and CNT hybrid reinforcement, J. Mater. Sci. 56 (2021) 3062–3077, https://doi.org/10.1007/s10853-020-05440-6.
[23] G. Song, L. Sun, S. Li, Y. Sun, Q. Fu, C. Pan, Synergistic effect of Gr and CNTs on preparing ultrathin Cu-(CNTs+Gr) composite foil via electrodeposition, Compos. Part B Eng. 187 (2020) 107841, https://doi.org/10.1016/j.compositesb.2020.107841.
[24] H. Yin, Q. Dai, X. Hao, W. Huang, X. Wang, Preparation and tribological properties of graphene oxide doped alumina composite coatings, Surf. Coat. Technol. 352 (2018) 411–419, https://doi.org/10.1016/j.surfcoat.2018.08.042.
[25] P. Wu, X. Chen, C. Zhang, J. Luo, Synergistic tribological behaviors of graphene oxide and nanodiamond as lubricating additives in water, Tribol. Int. 132 (2019) 177–184, https://doi.org/10.1016/j.triboint.2018.12.021.
[26] P. Maji, R.K. Nath, P. Paul, R.K. Bhogendro Meitei, S.K. Ghosh, Effect of processing speed on wear and corrosion behavior of novel MoS2 and CeO2 reinforced hybrid aluminum matrix composites fabricated by friction stir processing, J. Manuf. Process. 69 (2021) 1–11, https://doi.org/10.1016/j.jmapro.2021.07.032.
[27] H. Nautiyal, S. Kumari, R. Tyagi, U.S. Rao, O.P. Khatri, Evaluation of tribological performance of copper-based composites containing nano-structural 2D materials and their hybrid, Tribol. Int. 153 (2021) 106645, https://doi.org/10.1016/j.triboint.2020.106645.
[28] L. Kumar, S.K. Sahoo, S.N. Alam, Effect of xGnP/MWCNT reinforcement on mechanical, wear behavior and crystallographic texture of copper-based metal matrix composite, Mater. Sci. Eng. B Solid-State Mater. Adv. Technol. 263 (2021) 114888, https://doi.org/10.1016/j.mseb.2020.114888.
[29] L.L. Dong, Y.Q. Fu, Y. Liu, J.W. Lu, W. Zhang, W.T. Huo, L.H. Jin, Y.S. Zhang, Interface engineering of graphene/copper matrix composites decorated with tungsten carbide for enhanced physico-mechanical properties, Carbon N. Y. 173 (2021) 41–53, https://doi.org/10.1016/j.carbon.2020.10.091.
[30] T. Cetinkaya, S. Ozcan, M. Uysal, M.O. Guler, H. Akbulut, Free-standing flexible graphene oxide paper electrode for rechargeable Li-O2 batteries, J. Power Sources 267 (2014) 140–147, https://doi.org/10.1016/j.jpowsour.2014.05.081.
[31] F. Doğan, E. Duru, M. Uysal, H. Akbulut, S. Aslan, Tribology study of pulse electrodeposited Ni-B-SWCNT composite coating, JOM 74 (2022) 574–583, https://doi.org/10.1007/s11837-021-05070-6.
[32] Y.J. Li, X.T. Luo, C.J. Li, Dependency of deposition behavior, microstructure and properties of cold sprayed Cu on morphology and porosity of the powder, Surf. Coat. Technol. 328 (2017) 304–312, https://doi.org/10.1016/j.surfcoat.2017.08.070.
[33] L.N. Zhu, B.S. Xu, H.D. Wang, C.B. Wang, Determination of hardness of plasma-sprayed FeCrBSi coating on steel substrate by nanoindentation, Mater. Sci. Eng. A 528 (2010) 425–428, https://doi.org/10.1016/j.msea.2010.09.028.
[34] V. Mangam, S. Bhattacharya, K. Das, S. Das, Friction and wear behavior of Cu-CeO2 nanocomposite coatings synthesized by pulsed electrodeposition, Surf. Coat. Technol. 205 (2010) 801–805, https://doi.org/10.1016/j.surfcoat.2010.07.119.
[35] H. Zhang, N. Zhang, F. Fang, Fabrication of high-performance nickel/graphene oxide composite coatings using ultrasonic-assisted electrodeposition, Ultrason. Sonochem. 62 (2020) 104858, https://doi.org/10.1016/j.ultsonch.2019.104858.
[36] X. Tang, W. Yang, S. Yin, G. Tai, M. Su, J. Yang, H. Shi, D. Wei, J. Yang, Controllable graphene wrinkle for a high-performance flexible pressure sensor, ACS Appl. Mater. Interfaces 13 (2021) 20448–20458, https://doi.org/10.1021/acsami.0c22784.
[37] G. Lupina, M. Lukosius, J. Kitzmann, J. Dabrowski, A. Wolff, W. Mehr, Nucleation and growth of HfO2 layers on graphene by chemical vapor deposition, Appl. Phys. Lett. 103 (2013) 1–5, https://doi.org/10.1063/1.4828660.
[38] C. Liu, K. Wang, S. Luo, Y. Tang, L. Chen, Direct electrodeposition of graphene enabling the one-step synthesis of graphene-metal nanocomposite films, Small 7 (2011) 1203–1206, https://doi.org/10.1002/smll.201002340.
[39] B. Fang, D. Chang, Z. Xu, C. Gao, A review on graphene fibers: expectations, advances, and prospects, Adv. Mater. 32 (2020) 1–29, https://doi.org/10.1002/adma.201902664.
[40] A.J. Cobley, B. Abbas, A. Hussain, Improved electroless copper coverage at low catalyst concentrations and reduced plating temperatures enabled by low frequency ultrasound, Int. J. Electrochem. Sci. 9 (2014) 7795–7804.
[41] S. Ghosh, Electroless copper deposition: a critical review, Thin Solid Films 669 (2019) 641–658, https://doi.org/10.1016/j.tsf.2018.11.016.
[42] J.C. Patterson, C. Ni Dheasuna, J. Barrett, T.R. Spalding, M. O'Reilly, X. Jiang, G. M. Crean, Electroless copper metallisation of titanium nitride, Appl. Surf. Sci. 91 (1995) 124–128, https://doi.org/10.1016/0169-4332(95)00106-9.
[43] C. Zhang, D.M. Dabbs, L.M. Liu, I.A. Aksay, R. Car, A. Selloni, Combined effects of functional groups, lattice defects, and edges in the infrared spectra of graphene oxide, J. Phys. Chem. C 119 (2015) 18167–18176, https://doi.org/10.1021/acs.jpcc.5b02727.
[44] R.H. Guo, S.Q. Jiang, C.W.M. Yuen, M.C.F. Ng, An alternative process for electroless copper plating on polyester fabric, J. Mater. Sci. Mater. Electron. 20 (2009) 33–38, https://doi.org/10.1007/s10854-008-9594-4.
[45] X. Gan, Y. Wu, L. Liu, B. Shen, W. Hu, Electroless copper plating on PET fabrics using hypophosphite as reducing agent, Surf. Coat. Technol. 201 (2007) 7018–7023, https://doi.org/10.1016/j.surfcoat.2007.01.006.
[46] A. Joseph, B. Kirubasankar, A.M. Mathew, M. Narayanasamy, C. Yan, S. Angaiah, Influence of pulse reverse current parameters on electrodeposition of copper-graphene nanocomposite coating, Appl. Surf. Sci. Adv. 5 (2021) 100116, https://doi.org/10.1016/j.apsadv.2021.100116.
[47] S.S. Nanda, D.K. Yi, K. Kim, Study of antibacterial mechanism of graphene oxide using Raman spectroscopy, Sci. Rep. 6 (2016) 1–12, https://doi.org/10.1038/srep28443.
[48] J. Jiang, S. Zhang, P. Longhurst, W. Yang, S. Zheng, Molecular structure characterization of bituminous coal in northern China via XRD, Raman and FTIR spectroscopy, Spectrochim. Acta A Mol. Biomol. Spectrosc. 255 (2021) 119724, https://doi.org/10.1016/j.saa.2021.119724.
[49] Y. Lei, J. Jiang, T. Bi, J. Du, X. Pang, Tribological behavior of: in situ fabricated graphene-nickel matrix composites, RSC Adv. 8 (2018) 22113–22121, https://doi.org/10.1039/c8ra02510j.
[50] V. Khanna, V. Kumar, S.A. Bansal, Mechanical properties of aluminium- graphene/carbon nanotubes (CNTs) metal matrix composites: advancement, opportunities and perspective, Mater. Res. Bull. 138 (2021) 111224, https://doi.org/10.1016/j.materresbull.2021.111224.
[51] Y. Liu, F. Zheng, Y. Wu, C.C. Koch, P. Han, C. Zhang, Y. Liu, Y. Zhang, Grain refinement induced friction reduction and anti-wear performances of electrodeposited graphene/Ni composites with low content reduced graphene oxide, J. Alloys Compd. 826 (2020) 154080, https://doi.org/10.1016/j.jallcom.2020.154080.
[52] K.X. Wei, H.R. Zhou, F.L. Jia, K. Zhang, W. Wei, F.Q. Chu, D. Dan Wang, I. V. Alexandrov, Mechanical behaviors of graphene/copper matrix composite foils fabricated by pulse electrodeposition, Surf. Interfaces 24 (2021) 101142, https://doi.org/10.1016/j.surfin.2021.101142.
[53] Z. Guosong, C. Hongzhi, S. Xiaojie, T. Shuichang, S. Chunjian, Improvement of corrosion and wear resistance of Ni-W coatings by embedding graphene oxide modified by nano-Al2O3, J. Mater. Eng. Perform. 30 (2021) 7314–7327, https://doi.org/10.1007/s11665-021-05958-z.
[54] M. Uysal, H. Akbulut, M. Tokur, H. Algül, T. Çetinkaya, Structural and sliding wear properties of Ag/graphene/WC hybrid nanocomposites produced by electroless co-deposition, J. Alloys Compd. 654 (2016) 185–195, https://doi.org/10.1016/j.jallcom.2015.08.264.
[55] R.R.S. Santosh Singha, Suprakash Samantaa, Alok Kumar Dasb, Electrodeposited SiC-graphene oxide composite in nickel matrix for improved tribological applications, Surf. Topogr. Metrol. Prop. 2 (2020) 0–31.
[56] Z. Jia, T. Chen, J. Wang, J. Ni, H. Li, X. Shao, Synthesis, characterization and tribological properties of cu/reduced graphene oxide composites, Tribol. Int. 88 (2015) 17–24, https://doi.org/10.1016/j.triboint.2015.02.028.
[57] B.P. Singh, S. Nayak, K.K. Nanda, S. Bhattacharjee, L. Besra, B. Kumar, The production of a corrosion resistant graphene reinforced composite coating on copper by electrophoretic deposition, Carbon N. Y. 61 (2013) 47–56, https://doi.org/10.1016/j.carbon.2013.04.063.
[58] A. Aliyu, C. Srivastava, Correlation between growth texture, crystallite size, lattice strain and corrosion behavior of copper-carbon nanotube composite coatings, Surf. Coat. Technol. 405 (2021) 126596, https://doi.org/10.1016/j.surfcoat.2020.126596.
[59] Z. Gong, J. Shi, B. Zhang, J. Zhang, Graphene nano scrolls responding to superlow friction of amorphous carbon, Carbon N. Y. 116 (2017) 310–317, https://doi.org/10.1016/j.carbon.2017.01.106.
[60] J. Llorente, M. Belmonte, Rolled and twisted graphene flakes as self-lubricant and wear protecting fillers into ceramic composites, Carbon N. Y. 159 (2020) 45–50, https://doi.org/10.1016/j.carbon.2019.12.026.
[61] P. Li, L. Ji, H. Li, L. Chen, X. Liu, H. Zhou, J. Chen, Role of nanoparticles in achieving macroscale superlubricity of graphene/nano-SiO2 particle composites, Friction 10 (2022) 1305–1316, https://doi.org/10.1007/s40544-021-0532-2.
[62] A. Kamboj, Y. Raghupathy, M.Y. Rekha, C. Srivastava, Morphology, texture and corrosion behavior of nanocrystalline copper–graphene composite coatings, JOM 69 (2017) 1149–1154, https://doi.org/10.1007/s11837-017-2364-0.
[63] J. Cao, Q. Yang, L. Zhou, H. Chen, K. Zhan, J. Liu, R. Ding, S. You, B. Zhao, V. Ji, Microstructure, properties and synergetic effect of graphene oxide-functionalized carbon nanotubes hybrid reinforced copper matrix composites prepared by DC electrodeposition, Carbon N. Y. 212 (2023) 118157, https://doi.org/10.1016/j.carbon.2023.118157.
[64] K. Zhan, F. Li, J. Liu, J. Cao, Z. Wang, B. Zhao, Preparation and mechanism of Cu-GO laminated composite films with high thermal conductivity by intermediate nickel and silver layers via electrodeposition and ultrasonic spraying method, Surf. Coat. Technol. 472 (2023) 129960, https://doi.org/10.1016/j.surfcoat.2023.129960.